Available online at www.sciencedirect.com
ScienceDirect
Trans. Nonferrous Met. Soc. China 33(2023) 3295−3308
Transactions of Nonferrous Metals Society of China
www.tnmsc.cn

Microstructure evolution and strengthening mechanism of friction stir welded joint of 20 mm-thick AZ31 magnesium alloy

Qiang LIU[1], Wen WANG[1], Pai PENG[1], Ting ZHANG[1], Peng HAN[1],
Xiao-hu GUAN[1], Zhi WANG[1], Ke QIAO[1], Jun CAI[1], Kuai-she WANG[2]

1. School of Metallurgical Engineering, Xi'an University of Architecture and Technology, Xi'an 710055, China;
2. National and Local Joint Engineering Research Center for Functional Materials Processing, Xi'an University of Architecture and Technology, Xi'an 710055, China

Received 21 May 2022; accepted 16 September 2022

Abstract: A 20 mm-thick AZ31 Mg alloy plate was welded by friction stir welding, and the microstructure and mechanical properties of the joint were characterized in five layers along the thickness direction. The results showed that the grain size in the stir zone was uneven due to different welding temperatures and temperature drop rates. Different strong textures formed in different zones of the joint were mainly related to the material flow behavior. The yield strength and ultimate tensile strength (UTS) of the layered samples gradually increased from the top to the bottom surfaces of the joint. The elongation first increased from 9.5% to 10.5% and then decreased to 6.0% along the thickness of the joint. The UTS of the whole joint reached 88.5% that of the base material. The main strengthening mechanism of the joint was fine-grain strengthening.

Key words: microstructure evolution; mechanical properties; strengthening mechanism; friction stir welding; magnesium alloy; thick plate

1 Introduction

Magnesium (Mg) alloys have been widely used in aerospace, military equipment and railway industry owing to their low density, high specific strength and stiffness [1]. With the development requirements of lightweight, thick Mg alloy plates have attracted considerable attention. However, thick Mg alloy plates welded using traditional fusion welding technique are prone to generate defects, such as pores [2,3], hot cracks [4] and large distortion [5]. In particular, multi-pass fusion welding easily induces the formation of such defects, which severely impacts the mechanical properties of the joint [6]. Therefore, a new welding technique should be developed to realize high-quality joining of thick Mg alloy plates.

Friction stir welding (FSW) is a solid state welding technique [7], in which a high-speed rotating tool is used to soften and mix the materials, thus achieving welding [8,9]. Compared with traditional fusion welding technique, FSW exhibits many advantages, such as low heat input, no flux and low residual stress [10,11].

Currently, FSW has been successfully employed to weld thick aluminum (Al) alloy plates. It has been reported that the strength and joining efficiency of thick Al alloy plates welded using FSW were higher than those welded using fusion welding [12]. Until now, only thin Mg alloy plates have been successfully welded using FSW. There is a lack of research on welding thick Mg alloy plates using FSW. Compared with thin plates, thick Mg alloy plates welded using FSW should exhibit the following characteristics.

Corresponding author: Wen WANG, Tel: +86-13720527194, E-mail: wangwen2025@126.com;
Kuai-she WANG, Tel: +86-13186002826, E-mail: wangkuaishe888@126.com
DOI: 10.1016/S1003-6326(23)66334-4

Firstly, compared with the welding of thin plates, more heat input would be generated during the welding of thick Mg alloy plates with a large stir tool [13], According to previous research on the welding of thin Mg alloy plates, a high heat input yielded a larger grain size [14], which weakened fine-grain strengthening and reduced the mechanical properties of the joint [15]. However, whether this phenomenon will be observed in the FSW of thick Mg alloy plates needs to be experimentally verified.

Secondly, the grain orientation is one of the main factors that influence the mechanical properties of Mg alloy joints [16]. It was believed that the basal plane was distributed along the circumferential surface of the pin owing to the shearing effect of the stir tool during the FSW of thin Mg alloy plates [17,18]. For thick Mg alloy plates, a large strain gradient will be generated along the thickness of the joint, which may induce a new characteristic in the grain orientation.

Thirdly, an uneven microstructure inevitably occurs under significant temperature and strain gradients along the thickness of the FSW joint, which will affect the strength of the joint. For example, MAO et al [19] used FSW to weld thick AA7075-T6 alloy plates. They found that the microstructure along the thickness direction suffered from different thermal cycles, which led to considerable differences in the microstructure and mechanical properties of the layered samples. A similar phenomenon was also reported by ZHAO et al [20], who found that the FSW joint of thick 7N01 Al alloy plate exhibited low strength due to uneven microstructure and mechanical properties in the thickness direction. Based on the above consideration, in this study, it is necessary to focus on the uniformity of the microstructure and mechanical properties in the thickness direction of the joint. Moreover, it is also essential to establish the relationship between the microstructure and mechanical properties of the joint.

Therefore, in this study, a 20 mm-thick AZ31 Mg alloy plate was welded by FSW. The microstructure and mechanical properties of the joint were studied, and the welding temperature during FSW was measured. Moreover, the distribution characteristics of the grain size and the formation mechanism of the grain orientation along the thickness direction were revealed. The relationship between the microstructure and mechanical properties of the joint was established.

2 Experimental

In this study, hot-rolled plate of AZ31 Mg alloy with dimensions of 500 mm × 80 mm × 20 mm (length × width × thickness) was used as the base material (BM). FSW was performed using a FSW machine (FSW-LM-BM16) operated at a welding speed of 100 mm/min and a rotating speed of 400 r/min. The stir tool was made of H13 steel and composed of a concave double-ring shoulder with a diameter of 35 mm, a length of 19.7 mm right threaded tapered pin with diameters of 8.9 mm (the top) and 19.7 mm (the root). The tool tilt was set to be 3° at a plunge depth of 0.3 mm. The welding direction was parallel to the rolling direction of plates (Fig. 1(a)). WRNK−191 K-type

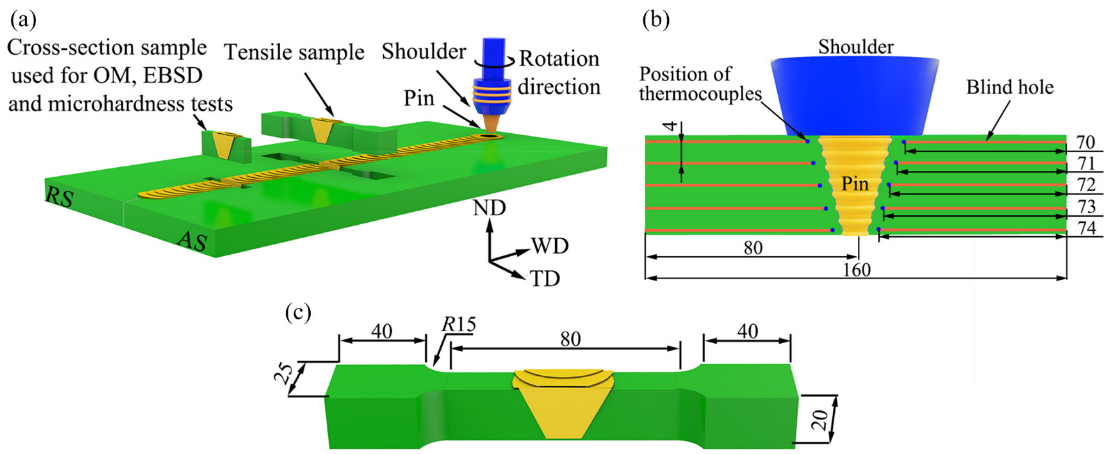

Fig. 1 Diagram of FSW process and sampling location (a), positions of blind holes for temperature measurement during FSW (b), and geometric parameters of tensile sample (c) (WD, TD and ND represent welding, transversal and normal directions, respectively; AS and RS represent advancing and retreading sides, respectively) (Unit: mm)

thermocouples were used to measure the temperature evolution during FSW. Five blind holes were prefabricated on the sides of two butting plates along the thickness direction, and the thermocouples were inserted into the blind holes (Fig. 1(b)).

After FSW, a metallographic sample with dimensions of 60 mm × 20 mm × 10 mm was cut along the transverse direction (TD) (Fig. 1(a)). After being mechanically ground and polished, the sample was etched with a corrosive liquid (1 mL nitric acid, 1 mL acetic acid, 1 g oxalic acid and 150 mL water) for 15 s. The cross-sectional macrostructure of the sample was observed by the optical microscopy (OM, Nikon SMZ 1000). The grain morphology and orientation were analyzed by scanning electron microscope (SEM, Zeiss Gemini SEM 300) equipped with an electron backscatter diffraction (EBSD, Oxford Nordlys Nano) tool. After mechanical polishing, the EBSD sample was electropolished using 10% alcohol perchlorate for 3 min at −30 °C and 12 V. For EBSD, the samples were subjected to a voltage of 20 kV at a working distance, step length and tilt angle of 14 mm, 0.7 μm and 70°, respectively. The dislocation density of the joint was analyzed by X-ray diffraction (XRD, D8 ADVANCE A25) and calculated by Eqs. (1) and (2) [21]:

$$\delta_{hkl}\cos\theta_{hkl}=\frac{\lambda}{D}+2\varepsilon\sin\theta_{hkl} \tag{1}$$

$$\rho_{\mathrm{Total}}=k_0\frac{\varepsilon^2}{b^2} \tag{2}$$

where δ_{hkl} is the half-height width of the modified XRD diffraction peak; θ_{hkl} is the Bragg angle; λ is the wavelength (0.154 nm); D is the grain size; ε is the internal strain; ρ_{Total} is the dislocation density; b is the amplitude of Burgers vector (0.32 nm); k_0 is a constant (which is equal to 1 for Mg alloys) [22].

A semi-automatic microhardness tester (401MVD) was used to perform microhardness test on the entire cross-section of the joint, in which the test interval was 1 mm, the load was 200 g, and dwell time was 15 s. Tensile samples were cut along the TD (Fig. 1(c)). To evaluate the tensile properties along the thickness direction, the tensile samples were divided into five layers, named Layers 1, 2, 3, 4 and 5 from the top to the bottom surfaces of the joint, respectively. The thickness of the layered tensile sample was 3.8 mm, and the other sizes were consistent with those of the sample in Fig. 1(c). Tensile tests were performed at room temperature using an electronic universal testing machine (CMT5205) at a tensile speed of 1 mm/min. All experiments were replicated three times to ensure the reliability of the experiments.

3 Results

3.1 Temperature fields

Figure 2 shows the schematic diagram of the temperature measurement positions and temperature curves during FSW. Along the horizontal direction, the peak temperature of the thermo-mechanically

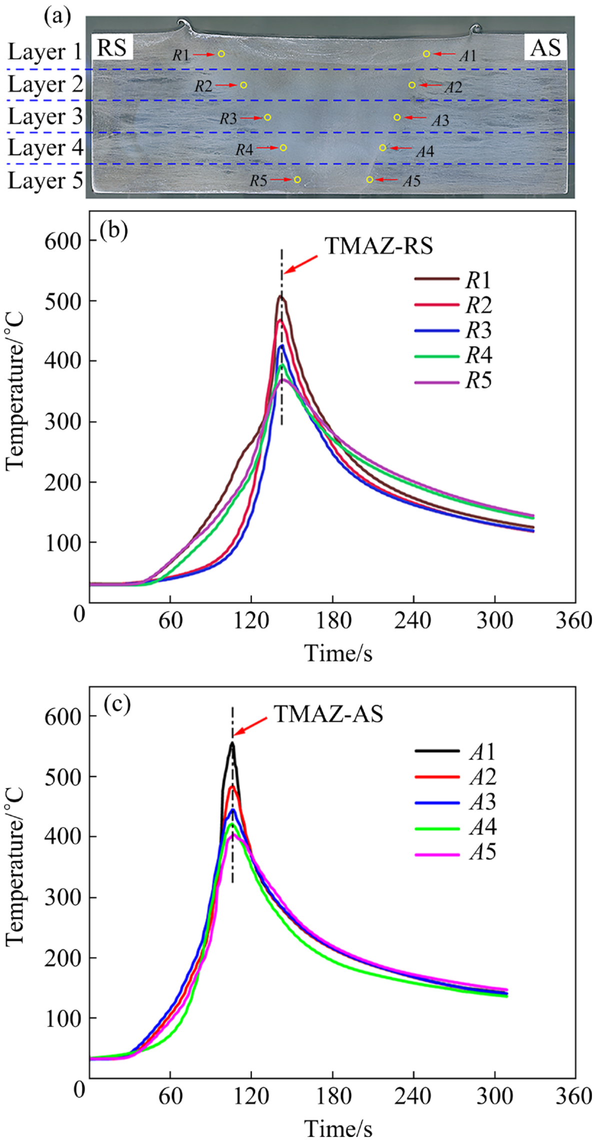

Fig. 2 Temperature measurement positions (a), and temperature curves in different thicknesses of joint (b, c) (Points $R1-R5$ are located in TMAZ-RS, and points $A1-A5$ are located in TMAZ-AS)

affected zone on the advancing side (TMAZ-AS) was higher than that in the thermo-mechanically affected zone on the retreading side (TMAZ-RS). The reason was that the material in the TMAZ-AS suffered greater shearing force and generated more frictional heat and deformation heat than that in the TMAZ-RS [19]. Similar result was also reported by ALBAKRI et al [23].

The welding temperature gradually decreased from Layer 1 to Layer 5 along the thickness direction. The peak temperatures of the TMAZ-AS and TMAZ-RS reduced from 556 to 404 °C and from 504 and 369 °C, respectively (Figs. 2(b) and (c)). This was because the heat input was mainly derived from the shoulder, and gradually decreased as it moved away from the shoulder. KIM et al [24] modelled the temperature distribution of a thin plate along the thickness direction during FSW. The results showed that the temperature distribution of the thin plate was similar to that of the thick plate, while the temperature difference (<40 °C) was small. In addition, the temperature drop rate of Layer 1 (Fig. 2(c)) was significantly faster than that of the other layers. This was because Layer 1 directly contacted with the atmosphere. In summary, the temperature distribution of FSW joints of thick Mg alloy plates along the horizontal and thickness directions was basically the same as that in the thin plates, whereas the temperature difference was considerably greater.

3.2 Macrostructure

Figure 3 shows the cross-sectional macrostructure of the joint, which shows no obvious defects such as micro-holes and cracks. Based on the microstructural characteristics, the joint can be divided into the stir zone (SZ), thermo-mechanically affected zone (TMAZ) and base metal (BM), whereas without obvious heat affected zone (HAZ). Moreover, an obvious shoulder effect zone at the top of the SZ (blue dashed line) can be observed, where the material underwent severe plastic deformation owing to the shearing effect of the shoulder.

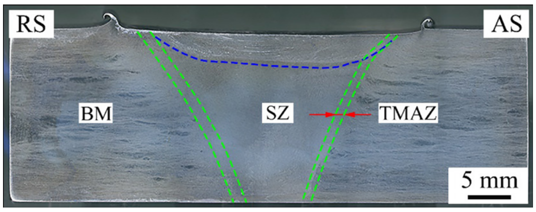

Fig. 3 Cross-sectional macrostructure of joint

3.3 Microstructure

Figure 4 shows the microstructure of the BM, which shows an obvious texture with an average grain size of 14.6 μm (Fig. 4(a)). The *c*-axis of grains was parallel to ND, indicating a typical rolled texture. The maximum pole density was 15.5 (Fig. 4(b)).

Figure 5 shows the grain morphologies in different zones of the joint. Along the horizontal direction, the grain size of the SZ from Layer 1 to Layer 4 was larger than those of the TMAZ and BM, which was inconsistent with the results reported by LI et al [25]. They found that the grain size of the SZ was smaller than those of the TMAZ and BM, attributing to the gradual decreasing degree of dynamic recrystallization from the SZ to TMAZ. Numerous studies had shown that the SZ grains of thin plate were significantly refined after FSW [26−28]. However, in this work, the grains of the SZ were coarsened. There were two main reasons for this phenomenon. Firstly, the heat input was excessively high during FSW of the thick Mg alloy plate, resulting in the grains coarsening.

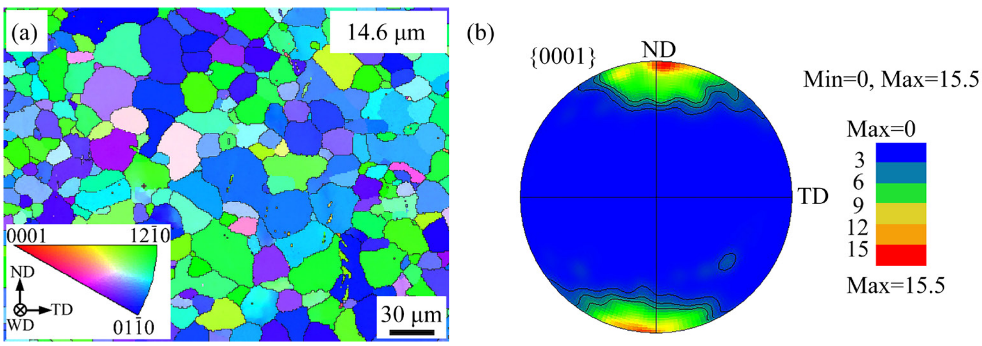

Fig. 4 Microstructure of BM: (a) Grain morphology; (b) Pole figure

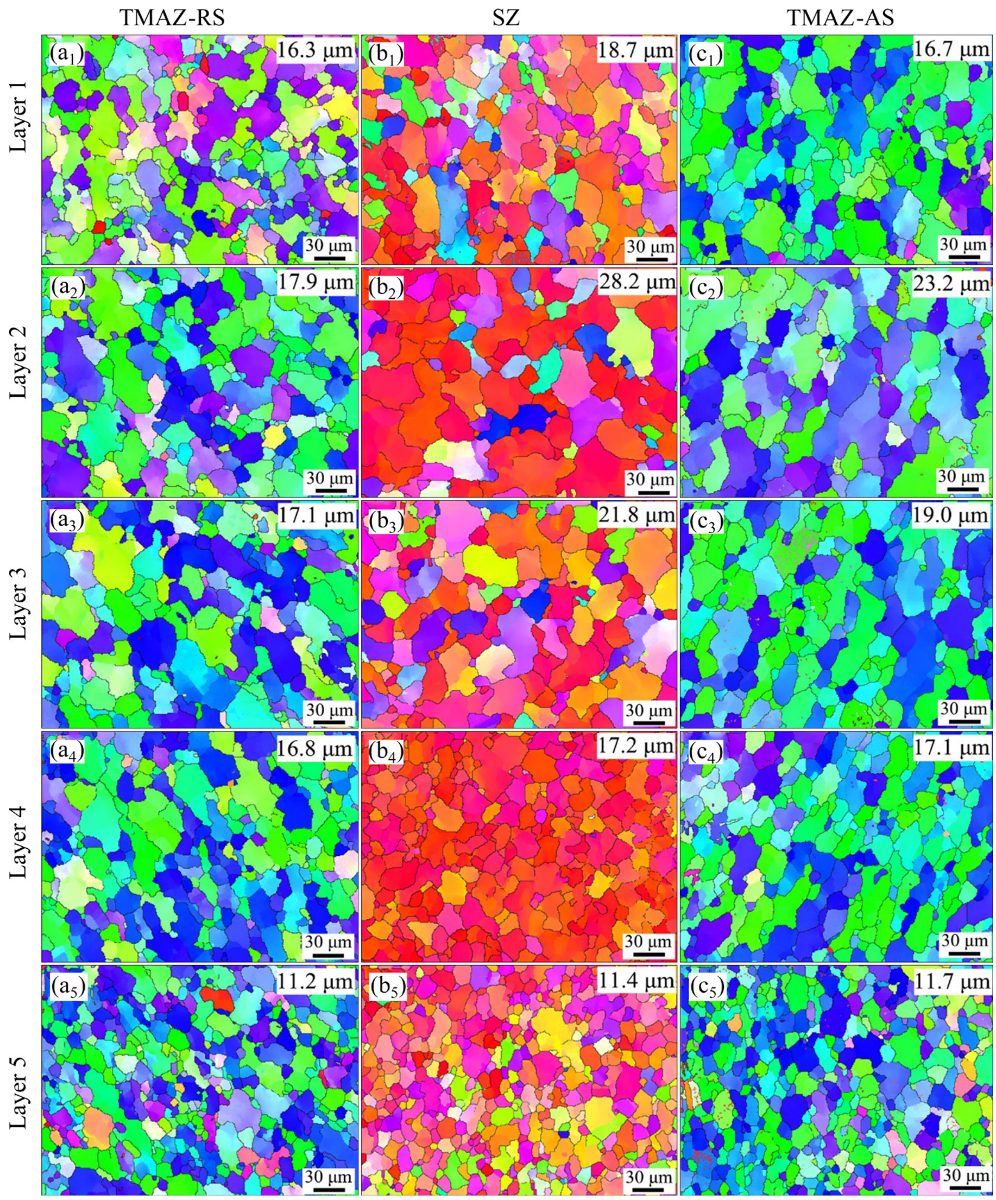

Fig. 5 Grain morphologies of different zones in each layer of joint: (a_1−a_5) TMAZ-RS; (b_1−b_5) SZ; (c_1−c_5) TMAZ-AS

Secondly, the heat dissipation rate of TMAZ was higher than that of the SZ along the horizontal direction. Moreover, Layer 5 had a lower heat input due to its larger distance from the shoulder, resulting in a smaller grain size of the SZ and TMAZ than that of BM (Figs. 5(a_5, b_5, c_5).

Comparatively, the grain size varied significantly along the thickness direction of the joint. The grain size of the SZ was 28.2 μm (Layer 2), 21.8 μm (Layer 3), 18.7 μm (Layer 1), 17.2 μm (Layer 4) and 11.4 μm (Layer 5). The grain size from Layer 2 to Layer 5 followed a rule that the lower the temperature was, the smaller the grain size was. According to the distribution of welding temperature (Fig. 2(b)), the temperature of Layer 2 was significantly lower than that of Layer 1 and the grain size of the former should have been smaller than that of the latter; however, the opposite result was observed. The main reasons for this are as follows. Firstly, the high strain rate triggered by the shoulder induced the grain refinement in Layer 1 [29]. Secondly, the cooling rate of Layer 1 was fast, inhibiting grain growth [30]. A similar grain evolution in the TMAZ was observed along the thickness direction.

Figure 6 shows the pole figures of the {0001} basal plane for different layers of the joint, which exhibits an obvious texture. In SZ, the *c*-axis of grains was tilted towards the WD by approximately 16°, 20° and 23° for Layers 2−4, respectively,

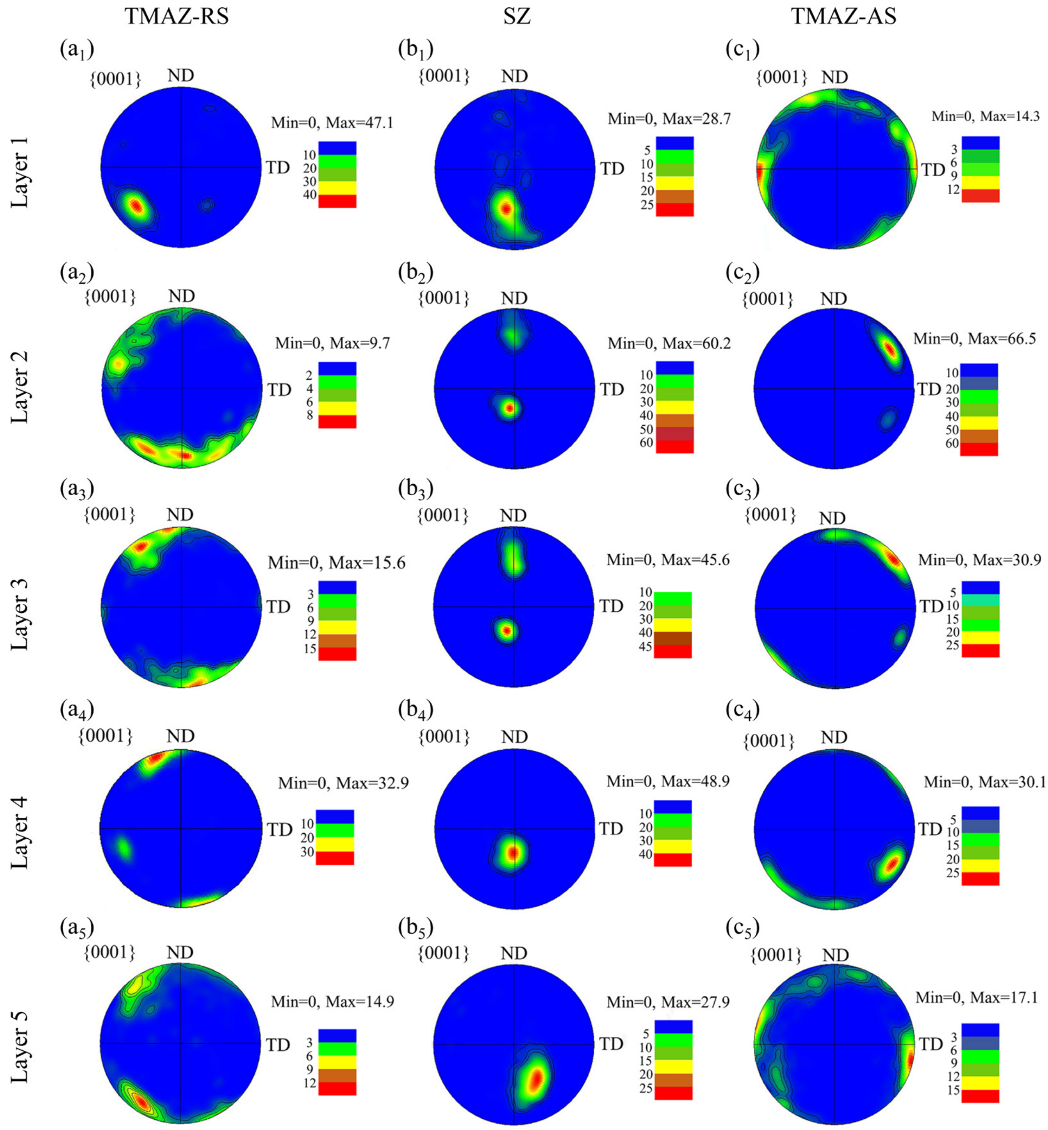

Fig. 6 Pole figures of different zones in each layer of joint: (a_1−a_5) TMAZ-RS; (b_1−b_5) SZ; (c_1−c_5) TMAZ-AS

almost perpendicular to the circumferential surface of the pin (Figs. 6(b_2−b_4)). Notably, the grain orientations of Layers 1 and 5 were different from those of the other layers, and the *c*-axis of grains deflected towards TD by 12° and 16°, respectively (Figs. 6(b_1) and (b_5)). Similar results were also reported by PARK et al [18]. Generally, the *c*-axis of grains was perpendicular to the circumferential surface of the pin, because the material underwent shear deformation, and the basal slip was activated during FSW. However, the grains of Layers 1 and 5 were constrained by the tool shoulder and backing plate, respectively, resulting in the deflection of the *c*-axis towards TD [18].

The angles between the *c*-axis of grains and the WD in the TMAZ-AS were 72°−85° (Figs. 6(c_1−c_5)), whereas those between the *c*-axis and the WD in the TMAZ-RS were 63°−81° (Figs. 6(a_1−a_5)). However, SHANG et al [31] reported that the angle between the *c*-axis and WD in the TMAZ-RS was 10°−90°, and the *c*-axis was roughly parallel to TD in the TMAZ-RS. They explained that the phenomenon was mainly related to the material flow under the shearing effect of the pin. The aforementioned results showed that the material flow of thick Mg plate in the TMAZ was different from that of a thin plate.

3.4 Mechanical properties

3.4.1 Microhardness

Figure 7 presents the microhardness distribution in the cross-section of the joint. The average micro-

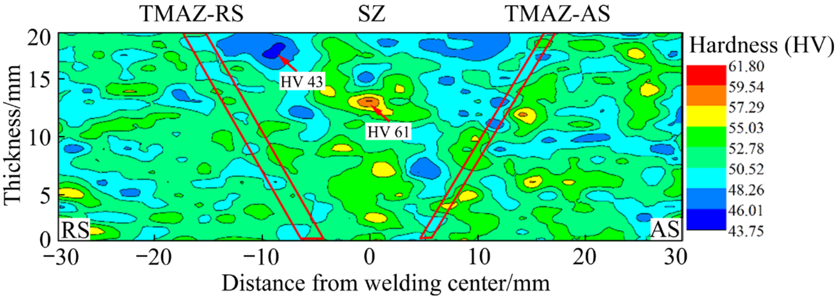

Fig. 7 Cross-sectional microhardness distribution of joint

hardness was HV 51 in BM, while SZ showed the highest microhardness value of HV 61. The microhardness gradually decreased away from the centre of the weld, and reached the lowest value of HV 43 near the TMAZ-RS. Similar result was also reported by XIN et al [32]. According to the Hall–Petch relationship, a small grain afforded high microhardness. In the present work, Layer 2 showed the largest grains (Fig. 5), whereas its microhardness was not the lowest. This was because that the basal slip was difficultly activated when the *c*-axis of grains was parallel or perpendicular to the force direction (Fig. 6(b_2)), resulting in high microhardness [33]. The above results indicated that the grain orientation strongly influenced the microhardness distribution in this study.

3.4.2 Tensile properties

Figure 8 shows the tensile properties of the BM, FSW joint and layered samples. The yield strength (YS) and ultimate tensile strength (UTS) of BM were 150 and 243 MPa, and those of the joint were 77 and 215 MPa, respectively. Compared with BM, the YS and UTS of the joint were reduced by 48.7% and 11.5%, respectively. There are two reasons for the decrease of the strength. On the one hand, the fine-grain strengthening effect was weakened due to grain coarsening. On the other hand, the inhomogeneous grain size and orientation along the thickness direction (Figs. 5 and 6) led to the uneven strength (Fig. 8). During tensile testing, local stress concentration was generated owing to uneven plastic deformation, which easily promoted the initiation of the cracks. The elongation (EL) of the joint (8.5%) was also considerably lower than that of BM (17.7%). Generally, a larger the grain size yielded a better EL of materials [34]. However, in this work, although the grain size of the joint was larger than that of BM, the EL was significantly

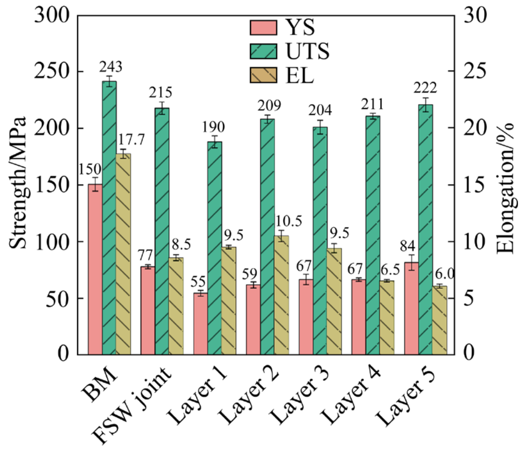

Fig. 8 Tensile properties of BM, FSW joint and layered samples

lower. This could be attributed to the strong basal texture of the joint [35].

The YS and UTS of the layered samples showed increasing trends along the thickness direction. The EL increased from 9.5% to 10.5% for Layers 1 to 2, and then gradually decreased to 6.0% for Layer 5. It is worth mentioning that both the YS and UTS of Layers 1−4 were lower than those of the joint, except for Layer 5. This indicated that Layers 1−4 caused lower joint strength. In particular, Layers 1 and 2 had the greatest effect on reducing the YS of the joint, Layers 1 and 3 had the greatest impact on reducing the UTS of the joint, and Layers 4 and 5 had the greatest effect on reducing the EI of the joint.

Figure 9 shows the macroscopic fracture morphologies of the BM and joint after tensile testing. The crack propagation path of BM sample followed a zigzag shape (Fig. 9(a)), which was attributed to the simultaneous occurrence of crack initiation and propagation at different locations during tensile testing. For the joint, the crack propagated along the TMAZ-AS (Fig. 9(b)) because the angle between the *c*-axis of grains and the tensile direction was approximately 45° in this region (Fig. 6), which resulted in the easy activation of the basal slip.

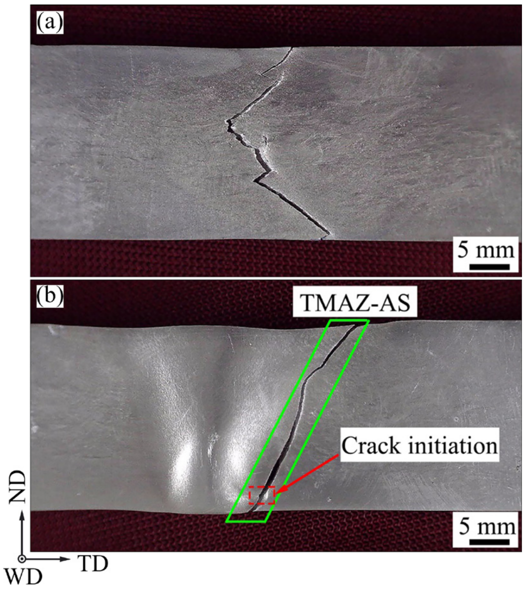

Fig. 9 Macroscopic fracture morphologies of tensile samples: (a) BM; (b) FSW joint

To verify the position of crack initiation, the strain hardening capacity of each layer can be calculated by Eq. (3) [36]:

$$H_c=\frac{\sigma_b-\sigma_y}{\sigma_y} \tag{3}$$

where H_c is the strain hardening capacity; σ_b and σ_y are the UTS and YS, respectively. The H_c values of Layers 1−5 were 2.5, 2.5, 2.0, 2.1 and 1.6, respectively. Compared with the other layers, Layer 5 showed the lowest H_c value, indicating that Layer 5 had the lowest strain hardening ability. It can also be observed that the crack initiated in Layer 5, as shown in red rectangle (Fig. 9(b)). Therefore, although Layer 5 showed the highest UTS and YS, it exhibited poor coordinated deformation ability during the tensile deformation, resulting in the occurrence of cracking. In summary, uneven plastic deformation caused by the microstructural inhomogeneity was the main reason for the premature failure of the joint.

4 Discussion

4.1 Microstructure evolution

4.1.1 Grain size evolution

The grain size was related to the welding temperature and strain rate. A high welding temperature and low strain rate usually generate a larger grain size [14]. The Zener–Holloman parameter (Z) reflects the combined effects of the welding temperature and strain rate on the grain size [29]. Consequently, the quantitative relationship between the grain size and the Z parameter was established by Eqs. (4) and (5) [37−39]:

$$Z=\dot{\varepsilon}\exp\left(\frac{Q}{RT}\right) \tag{4}$$

$$Zd^{m_1}=A \tag{5}$$

where Z is the Zener–Holloman parameter; $\dot{\varepsilon}$ represents the strain rate; Q is the lattice diffusion activation energy (135 kJ/mol [29]); R is the molar gas constant (8.314 J/(mol·K)); T is the peak temperature of SZ during FSW; d is the grain size; m_1 is the grain size index; A is a constant.

Since the peak temperature of SZ could not be measured, the average value of the peak temperatures of TMAZ-AS and TMAZ-RS was used as the peak temperature of the SZ. The strain rate was calculated by the equation $\dot{\varepsilon}=(R_m\cdot 2\pi r_e)/L_e$, where R_m was the average flow rate of the material, which was assumed to be half of the rotation speed (200 r/min) [37]; r_e and L_e were the effective radius and thickness of the dynamic recrystallization areas of different layers respectively, which could be calculated as 0.78 times the boundary radius and thickness of the recrystallization areas [14]. The r_e values of Layers 1−5 were 11.0, 8.5, 6.5, 4.7 and 3.3 mm, respectively, and the L_e is 3.1 mm.

Figure 10 shows the relationship between the grain size and the Z parameter, revealing that the larger the Z value was, the smaller the grain size was. The quantitative relationship between the grain size d and the Z parameter in the SZ for Layers 2−5 was obtained by linear fitting as follows:

$$\ln d=14.85-0.44\ln Z \tag{6}$$

It should be noted that the relationship between the grain size and the Z parameter in the SZ for Layer 1 did not accord with this law due to a fast cooling rate.

The above studies showed that a low welding temperature and a high strain rate could increase the Z value and thus refine grains. The strain rates of Layers 2−5 were 114, 87, 63 and 44 s^{-1}, respectively, showing a gradual decreasing trend. In general, grain size should be gradually coarsened, which was contrary to the actual result. However, the variation of temperature was consistent with that of grain size, which indicated that the influence of the temperature on the grain size was greater than that of the strain rate during FSW. Similar result has been reported by ZHANG and WU [40].

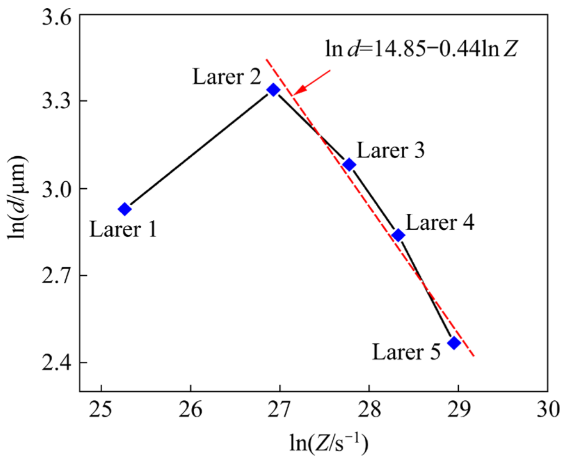

Fig. 10 Relationship between grain size and Z parameter in different layers of joint

4.1.2 Texture evolution

Previous studies showed that the plastic deformation was mainly affected by the shearing action of the stir pin during FSW of thin Mg plates [18]. Under the condition of plastic deformation mechanism dominated by basal slip, the basal plane underwent shear deformation along the circumference of the stir pin, resulting in the basal plane parallel to the circumference of the stir pin (shear surface), and the c-axis perpendicular to the rotation direction of the stir pin (shear direction) [17]. To clarify the relationship between the grain orientation and shear deformation in this study, the grain orientation was transformed from the sample coordinate system to the shear coordinate system (comprising the shear plane and shear direction), as shown in Fig. 11. The sample and shear coordinate systems were denoted as CS_1: X_1, Y_1, Z_1 and CS_0: X_0, Y_0, Z_0, respectively.

Figure 12 shows the pole figures of different zones in each layer under the shear coordinate system. In the SZ, the grain orientation basically followed the distribution characteristics induced by the shearing action. The basal plane was roughly parallel to the shear plane, and the c-axis was perpendicular to the shear direction. However, the grain orientation of Layers 1 and 5 showed a certain deviation from the above phenomenon, in which the angles between the basal plane and the shear plane were 20°−30°, and those between the c-axis and the shear direction were 70°−80°. This was because Layer 1 was not only sheared by the pin, but also sheared and squeezed by the tool shoulder, and Layer 5 experienced shearing by the pin and constraint effect of the backing plate [18].

In the TMAZ, the grain orientation was different from that induced by pure shearing. The c-axis of grains in the TMAZ-AS was basically perpendicular to the shear direction, whereas the basal plane was deflected by a certain angle relative to the shear plane (Figs. 12(c_1−c_5)). This indicated that the plastic flow behaviour of the materials in the TMAZ-AS during FSW thick Mg plate was different from that of the thin plate. The pin used for welding the thick plate was obviously larger than that used for welding the thin plate, and the thread depth was also increased. Due to the increased thread depth and the 3° inclination of the tool, the material in the TMAZ-AS flowed vertically along the thickness direction [41,42], resulting in the deflection of the basal plane of grains relative to the shear plane. There was no obvious regularity in the grain orientation of the TMAZ-RS. In general, the material in the front of the pin is usually squeezed from AS to RS during FSW [43]. During FSW of thick Mg alloy plate, the amount of the material driven by each rotation of the pin was much greater than that of the thin plate, which caused extrusion degree of thick plate to be

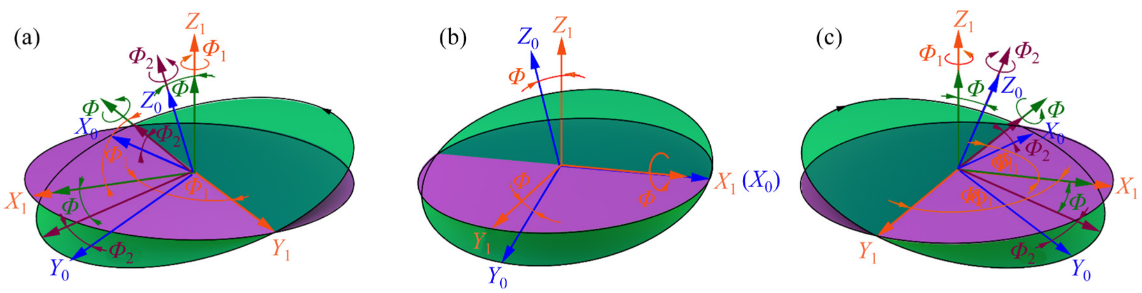

Fig. 11 Relationship between CS_0 and CS_1 of different zones in joint: (a) TMAZ-RS; (b) SZ; (c) TMAZ-AS

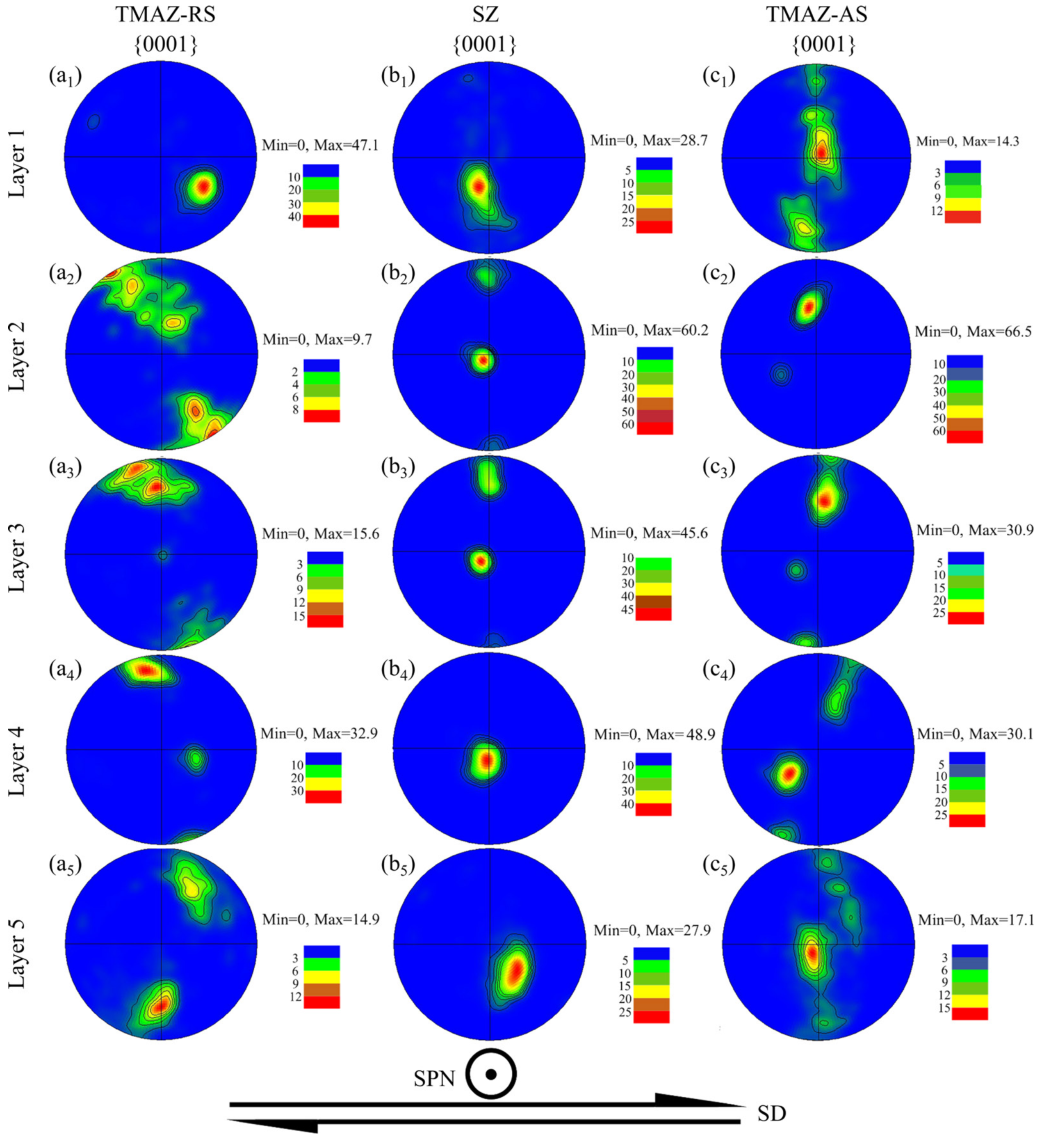

Fig. 12 Pole figures of different zones in each layer of joint under shear plane and shear direction coordinates: (a_1−a_5) TMAZ-RS; (b_1−b_5) SZ; (c_1−c_5) TMAZ-AS (SPN and SD represent the shear plane normal direction and shear direction, respectively)

greater than that of thin plate in the TMAZ-RS. Moreover, the material in the TMAZ-RS also underwent vertical flow, and the plastic flow mode was more complicated, which made the grain orientation distribution different from that of pure shear.

In summary, the grain orientation evolution of FSW thick Mg alloy plate was not only affected by the shearing of the pin, but also by the vertical and horizontal flow of the material.

4.2 Relationship between microstructure and tensile properties

The strengthening mechanisms of AZ31 Mg alloy mainly included grain boundary strengthening, texture strengthening and dislocation strengthening [22,44,45]. To clarify the influence of the microstructure on the tensile properties, the contribution of the grain boundary strengthening, texture strengthening and dislocation strengthening to the YS of the joint was quantitatively analyzed by Eqs. (7)−(10) [21]:

$$\sigma_y=\sigma_{gbs}+\sigma_{ts}+\sigma_{ds} \tag{7}$$

$$\sigma_{gbs}=\sigma_0+k_1 d^{-1/2} \tag{8}$$

$$\sigma_{ts}=\tau_0/m \tag{9}$$

$$\sigma_{ds}=\alpha G b\sqrt{\rho_{Total}} \tag{10}$$

where σ_y is the yield strength, σ_{gbs}, σ_{ts} and σ_{ds} are the contributions of grain boundary strengthening, texture strengthening and dislocation strengthening to the YS, respectively; σ_0 is the lattice friction resistance (10 MPa [35]); k_1 is the stress concentration factor (157 MPa·μm$^{1/2}$ [46]); τ_0 is the critical shear stress of the basal slip system (5.24 MP [47]); m is the Schmid factor; α is a constant (0.2); G is the shear modulus (17000 MPa); b is equal to 0.32 nm [48]; ρ_{Total} is calculated using Eqs. (1) and (2). The dislocation densities of Layers 1−5 were 1.54×10^{14}, 1.53×10^{14}, 1.47×10^{14}, 1.38×10^{14} and 1.15×10^{14} m^{-2}, respectively.

The contributions of the various strengthening mechanisms of the layers to the YS were calculated by Eqs. (7)−(10), and the results are shown in Table 1. It can be seen that the main strengthening mechanism was grain boundary strengthening. However, LI and LI [44] found that the main strengthening mechanism of the AZ31 Mg alloy was texture strengthening after a large pre-compression deformation. The reason was that the c-axis of grains was parallel to the compression direction, the Schmidt factor was small, and the basal slip was difficult to activate, which increased the effect of texture strengthening. In this work, the angle between the c-axis of grains in the TMAZ-AS and the tensile direction was nearly 45°, and the basal slip was activated easily. This indicated that strong soft orientation texture was formed in the joint, which deteriorated the joint strength.

Table 1 Contributions of various strengthening mechanisms in different layers of joint to YS

Parameter	Strengthening contribution/MPa				
	Layer 1	Layer 2	Layer 3	Layer 4	Layer 5
σ_{gbs}	48	42	46	47	54
σ_{ts}	18	12	17	13	17
σ_{ds}	13	13	13	12	11
Calculated σ_y	79	67	76	72	82
Experimental σ_y	55	59	67	67	84
$\lvert\sigma_{y,cal.}-\sigma_{y,exp.}\rvert$	24	8	9	5	2

Along the thickness direction, the difference of grain size in the SZ was 16.8 μm (Fig. 5), which was twice that of the thin plate (7.4 μm) [16]. This induced that the difference in the contribution of grain boundary strengthening to the YS was 12 MPa, which accounted for 22% of the lowest YS (55 MPa) of the layered samples. In addition, the grain orientation and maximum pole density of each layer also simultaneously showed large differences along the thickness direction (Fig. 6). This resulted in that the difference in the contribution of texture strengthening to the YS accounted for 11% of the lowest YS of the layered samples. The aforementioned results showed that the uneven microstructure led to the uneven distribution of the mechanical properties of the joint. During the tensile process, the plastic deformation of the joint was uneven, which induced low joint strength.

In summary, the main strengthening mechanism for FSW joint of the thick Mg alloy plate was grain boundary strengthening. The soft orientation and uneven microstructure along the thickness direction were the main factors that reduced the mechanical properties of the joint. The strength and plasticity of the joint can be improved by refining grains, strengthening grain orientation, and improving microstructure uniformity by means of optimizing welding process in the future.

5 Conclusions

(1) The grain size of FSW thick Mg alloy plate joint was obviously different from that of the thin plate. The grains in the SZ were larger than those in the TMAZ and BM for Layers 1−4. The grain size gradually decreased along the thickness direction, except for Layer 1. The grain size was mainly affected by the welding temperature and strain rate, and the welding temperature has the greatest influence on the grain size.

(2) In the SZ, the c-axis of grains was roughly perpendicular to the TD, and the grain orientation basically followed the distribution characteristics caused by the pure shearing deformation. The angles between the c-axis and the WD were 72°–85° in the TMAZ-AS, and those between the c-axis and the WD were 63°–81° in the TMAZ-RS. The grain orientation evolution was not only affected by the shearing of the stir pin, but also by the vertical and horizontal flow of the materials.

(3) After FSW, the highest microhardness was observed in the SZ center. The YS, UTS and EL of the FSW joint were lower than those of BM, and the UTS of the joint reached 88.5% that of BM. The YS and UTS of layered samples gradually increased

along the thickness direction, and the EL first increased and then decreased gradually.

(4) The main strengthening mechanism of FSW joint was grain boundary strengthening. The soft orientation was the main factor for the loss of the strength, while the microstructure inhomogeneity was the main reason for the loss of the ductility.

Acknowledgments

The authors gratefully acknowledge the sponsorship from the State Key Program of National Natural Science Foundation of China (Nos. U1760201, 52034005), the National Natural Science Foundation of China (No. 51974220), the Key Research and Development Program of Shaanxi Province, China (Nos. 2020ZDLGY13-06, 2017ZDXM-GY-037), the Innovation Capacity Support Project of Shaanxi Province, China (No. 2020KJXX-077), and the Education Department Foundation of Shaanxi Province, China (No. 17JK0430).

References

[1] HU Jian-jun, LIAO Jing, YANG Xian, ZENG Jing, LI Hui, SONG Bo, XU Hong-bin, GUO Ning, JIN Yan. Microstructure and properties of Al-coating on AZ31 magnesium alloy prepared by pack-cementation [J]. Transactions of Nonferrous Metals Society of China, 2022, 32: 493−502.

[2] LI G H, ZHOU L, ZHANG H F, GUO G Z, LUO S F, GUO N. Evolution of grain structure, texture and mechanical properties of a Mg−Zn−Zr alloy in bobbin friction stir welding [J]. Materials Science and Engineering A, 2021, 799: 140267.

[3] YANG Xia-wei, FENG Wu-yuan, LI Wen-ya, DONG Xiu-rong, XU Ya-xin, CHU Qiang, YAO Shuo-tian. Microstructure and properties of probeless friction stir spot welding of AZ31 magnesium alloy joints [J]. Transactions of Nonferrous Metals Society of China, 2019, 29: 2300−2309.

[4] LI Gao-hui, ZHOU Li, ZHANG Jun-feng, LUO San-feng, GUO Ning. Macrostructure, microstructure and mechanical properties of bobbin tool friction stir welded ZK60 Mg alloy joints [J]. Journal of Materials Research and Technology, 2020, 9: 9348−9361.

[5] DHARANI KUMAR S, SURESH KUMAR S. Effect of heat treatment conditions on ballistic behaviour of various zones of friction stir welded magnesium alloy joints [J]. Transactions of Nonferrous Metals Society of China, 2021, 31: 156−166.

[6] ZHANG Zhi-hui, DONG Shi-yun, WANG Yu-jiang, XU Bin-shi, FANG Jin-xiang, HE Peng. Microstructure characteristics of thick aluminum alloy plate joints welded by fiber laser [J]. Materials & Design, 2015, 84: 173−177.

[7] BARADARANI F, MOSTAFAPOUR A, SHALVANDI M. Effect of ultrasonic assisted friction stir welding on microstructure and mechanical properties of AZ91−C magnesium alloy [J]. Transactions of Nonferrous Metals Society of China, 2019, 29: 2514−2522.

[8] HUANG Yong-xian, MENG Xiang-chen, XIE Yu-ming, WAN Long, LV Zong-liang, CAO Jian, FENG Ji-cai. Friction stir welding/processing of polymers and polymer matrix composites [J]. Composites (Part A): Applied Science and Manufacturing, 2018, 105: 235−257.

[9] ABBASI M, BAGHERI B, SHARIFI F. Simulation and experimental study of dynamic recrystallization process during friction stir vibration welding of magnesium alloys [J]. Transactions of Nonferrous Metals Society of China, 2021, 31: 2626−2650.

[10] LIU Zhe, XIN Ren-long, WU Xia, LIU De-jia, LIU Qing. Improvement in the strength of friction-stir-welded ZK60 alloys via post-weld compression and aging treatment [J]. Materials Science and Engineering A, 2018, 712: 493−501.

[11] SINGH K, SINGH G, SINGH H. Investigation of microstructure and mechanical properties of friction stir welded AZ61 magnesium alloy joint [J]. Journal of Magnesium and Alloys, 2018, 6: 292−298.

[12] MAO Yu-qing, KE Li-ming, CHEN Yu-hua, LIU Fen-cheng, XING Li. Inhomogeneity of microstructure and mechanical properties in the nugget of friction stir welded thick 7075 aluminum alloy joints [J]. Journal of Materials Science & Technology, 2018, 34: 228−236.

[13] SCHMIDT H, HATTEL J, WERT J. An analytical model for the heat generation in friction stir welding [J]. Modelling and Simulation in Materials Science and Engineering, 2004, 12: 143−157.

[14] CHANG C I, DU X H, HUANG J C. Achieving ultrafine grain size in Mg−Al−Zn alloy by friction stir processing [J]. Scripta Materialia, 2007, 57: 209−212.

[15] MIRONOV S, ONUMA T, SATO Y S, KOKAWA H. Microstructure evolution during friction-stir welding of AZ31 magnesium alloy [J]. Acta Materialia, 2015, 100: 301−312.

[16] YANG J, WANG D, XIAO B L, NI D R, MA Z Y. Effects of rotation rates on microstructure, mechanical properties, and fracture behavior of friction stir-welded (FSW) AZ31 magnesium alloy [J]. Metallurgical and Materials Transactions A, 2013, 44: 517−530.

[17] SHANG Q, NI D R, XUE P, XIAO B L, MA Z Y. Improving joint performance of friction stir welded wrought Mg alloy by controlling non-uniform deformation behavior [J]. Materials Science and Engineering A, 2017, 707: 426−434.

[18] PARK S H C, SATO Y S, HIROYUKI K. Basal plane texture and flow pattern in friction stir weld of a magnesium alloy [J]. Metallurgical and Materials Transactions A, 2003, 34: 987−994.

[19] MAO Yu-qing, KE Li-ming, LIU Fen-cheng, CHEN Yu-hua, XING Li. Investigations on temperature distribution, microstructure evolution, and property variations along thickness in friction stir welded joints for thick AA7075-T6 plates [J]. The International Journal of Advanced Manufacturing Technology, 2016, 86: 141−154.

[20] ZHAO Ying-xin, YANG Zhi-yong, DOMBLESKY J P, HAN Jian-min, LI Zhi-qiang, LIU Xiao-long. Investigation of through thickness microstructure and mechanical properties in friction stir welded 7N01 aluminum alloy plate [J]. Materials Science and Engineering A, 2019, 760: 316−327.

[21] PENG Pai, WANG Kuai-she, WANG Wen, HAN Peng, ZHANG Ting, LIU Qiang, ZHANG Sheng-yi, WANG Hong-duo, QIAO Ke, LIU Jian. Relationship between microstructure and mechanical properties of friction stir processed AISI 316 Relationship between microstructure and mechanical properties of friction stir processed AISI 316L steel produced by selective laser melting [J]. Materials Characterization, 2020, 163: 110283.

[22] ROODPOSHTI P S, SARKAR A, MURTY K L, SCATTERGOOD R O. Dislocation density evolution during creep of AZ31 Mg alloy: A study by X-ray diffraction line profile analysis [J]. Metallography, Microstructure, and Analysis, 2015, 4: 337−343.

[23] ALBAKRI A N, MANSOOR B, NASSAR H, KHRAISHEH M K. Thermo-mechanical and metallurgical aspects in friction stir processing of AZ31 Mg alloy—A numerical and experimental investigation [J]. Journal of Materials Processing Technology, 2013, 213: 279−290.

[24] KIM D, BADARINARAYAN H, KIM J H, KIM C, OKAMOTO K, WAGONER R H, CHUNG K. Numerical simulation of friction stir butt welding process for AA5083-H18 sheets [J]. European Journal of Mechanics, 2010, 29: 204−215.

[25] LI Ya-jie, QIN Feng-ming, LIU Cui-rong, LI Lei-jun, ZHAO Xiao-dong, WU Zhi-sheng. Influence of annealing treatment on microstructure evolution and mechanical property of friction stir weld AZ31 Mg alloys [J]. Journal of Wuhan University of Technology: Mater Sci Ed, 2019, 34: 417−425.

[26] HARIKRISHNA K L, DILIP J J S, CHOUDARY K R, RAO V V S, RAO S R K, RAM G D J, SRIDHAR N, REDDY G M. Friction stir welding of magnesium alloy ZM21 [J]. Transactions of the Indian Institute of Metals, 2010, 63: 807−811.

[27] XIN Ren-long, LI Bo, LIU Qing. Microstructure and texture evolution during friction stir processing of AZ31 Mg alloy [J]. Materials Science Forum, 2010, 654/655/656: 1195−1200.

[28] WANG Wen, YUAN Sheng-nan, QIAO Ke, WANG Kuai-she, ZHANG Sheng-yi, PENG Pai, ZHANG Ting, PENG Han, WU Bing, YANG Juan. Microstructure and nanomechanical behavior of friction stir welded joint of 7055 aluminum alloy [J]. Journal of Manufacturing Processes, 2021, 61: 311−321.

[29] CHANG C I, LEE C J, HUANG J C. Relationship between grain size and Zener–Holloman parameter during friction stir processing in AZ31 Mg alloys [J]. Scripta Materialia, 2004, 51: 509−514.

[30] WANG Jian, LU Ya-lin, ZHOU Dong-shuai, ZHANG Yang, BAI Zhi-hao, LI Xing-cheng. Effects of cooling condition on microstructural evolution and mechanical properties of friction stir processed 2A14 aluminum alloy [J]. Materials Research Express, 2019, 6: 126577.

[31] SHANG Q, NI D R, XUE P, XIAO B L, MA Z Y. Evolution of local texture and its effect on mechanical properties and fracture behavior of friction stir welded joint of extruded Mg−3Al−1Zn alloy [J]. Materials Characterization, 2017, 128: 14–22.

[32] XIN Ren-long, LI Bo, LIAO Ai-lin, ZHOU Zheng, LIU Qing. Correlation between texture variation and transverse tensile behavior of friction-stir-processed AZ31 Mg alloy [J]. Metallurgical and Materials Transactions A, 2012, 43: 2500−2508.

[33] PENG Jin-hua, ZHANG Zhen, LIU Zhao, LI Yao-zu, GUO Peng, ZHOU Wei, WU Yu-cheng. The effect of texture and grain size on improving the mechanical properties of Mg−Al−Zn alloys by friction stir processing [J]. Scientific Reports, 2018, 8: 4196.

[34] YUAN W, MISHRA R S. Grain size and texture effects on deformation behavior of AZ31 magnesium alloy [J]. Materials Science and Engineering A, 2012, 558: 716−724.

[35] WANG Y N, CHANG C I, LEE C J, LIN H K, HUANG J C. Texture and weak grain size dependence in friction stir processed Mg−Al−Zn alloy [J]. Scripta Materialia, 2006, 55: 637−640.

[36] AFRIN N, CHEN D L, CAO X, JAHAZI M. Strain hardening behavior of a friction stir welded magnesium alloy [J]. Scripta Materialia, 2007, 57: 1004−1007.

[37] RAZMPOOSH M H, ZAREI-HANZAKI A, IMANDOUST A. Effect of the Zener–Hollomon parameter on the microstructure evolution of dual phase TWIP steel subjected to friction stir processing [J]. Materials Science and Engineering A, 2015, 638: 15−19.

[38] SINGH V, MONDAL C, SARKAR R, BHATTACHARJEE P P, GHOSAL P. Dynamic recrystallization of a β(B2)-stabilized γ-TiAl based Ti−45Al−8Nb−2Cr−0.2B alloy: The contributions of constituent phases and Zener−Hollomon parameter modulated recrystallization mechanisms [J]. Journal of Alloys and Compounds, 2020, 828: 154386.

[39] XU Nan, FENG Ruo-nan, GUO Wen-feng, SONG Qi-ning, BAO Ye-feng. Effect of Zener–Hollomon parameter on microstructure and mechanical properties of copper subjected to friction stir welding [J]. Acta Metallurgica Sinica (English Letters), 2020, 33: 319−326.

[40] ZHANG Zhao, WU Qi. Numerical studies of tool diameter on strain rates, temperature rises and grain sizes in friction stir welding [J]. Journal of Mechanical Science and Technology, 2015, 29: 4121−4128.

[41] MORISADA Y, IMAIZUMI T, FUJII H. Clarification of material flow and defect formation during friction stir welding [J]. Science and Technology of Welding and Joining, 2015, 20: 130−137.

[42] ZHANG Z, XIAO B L, WANG D, MA Z Y. Effect of alclad layer on material flow and defect formation in friction-stir-welded 2024 aluminum alloy [J]. Metallurgical and Materials Transactions A, 2011, 42: 1717−1726.

[43] ZENG X H, XUE P, WANG D, NI D R, XIAO B L, MA Z Y. Effect of processing parameters on plastic flow and defect formation in friction-stir-welded aluminum alloy [J]. Metallurgical and Materials Transactions A, 2018, 49: 2673−2683.

[44] LI Xin-feng, LI Qi-zhen. Effect of pre-compression on

microstructural evolution, mechanical property and strengthening mechanism of AZ31 alloy [J]. Journal of Materials Science, 2020, 55: 11637−11649.
[45] BARNETT M R, KESHAVARZ Z, BEER A G, ATWELL D. Influence of grain size on the compressive deformation of wrought Mg−3Al−1Zn [J]. Acta Materialia, 2004, 52: 5093−5103.
[46] WANG Ling, ZHAO Yi-quan, ZHANG Jing, MA Ru, LIU Yan-dong, WANG Yi-nong, ZHANG Qun, LI Wei-gang, ZHANG Yuan. Quantitative analysis on friction stress of hot-extruded AZ31 magnesium alloy at room temperature [J]. Journal of Materials Science & Technology, 2018, 34: 1765−1772.
[47] RAEISINIA B, AGNEW S R, AKHTAR A. Incorporation of solid solution alloying effects into polycrystal modeling of Mg alloys [J]. Metallurgical and Materials Transactions A, 2011, 42: 1418−1430.
[48] ZENG Z R, ZHU Y M, NIE J F, XU S W, DAVIES C H J, BIRBILIS N. Effects of calcium on strength and microstructural evolution of extruded alloys based on Mg−3Al−1Zn−0.3Mn [J]. Metallurgical and Materials Transactions A, 2019, 50: 4344−4363.

20 mm 厚 AZ31 镁合金厚板搅拌摩擦焊接接头的显微组织演变及强化机制

刘 强[1]，王 文[1]，彭 湃[1]，张 婷[1]，韩 鹏[1]，关肖虎[1]，王 智[1]，乔 柯[1]，蔡 军[1]，王快社[2]

1. 西安建筑科技大学 冶金工程学院，西安 710055；
2. 西安建筑科技大学 功能材料加工国家地方联合工程研究中心，西安 710055

摘 要：采用搅拌摩擦焊焊接 20 mm 厚 AZ31 镁合金板材，并沿厚度方向分 5 层对接头的显微组织和力学性能进行表征。结果表明：焊接温度和温降速率的不同导致搅拌区晶粒尺寸不均匀，且在材料流动行为的作用下，接头不同区域形成不同强织构。此外，接头各层的屈服强度和抗拉强度从上表面至下表面整体呈逐渐增加的趋势，伸长率沿接头厚度方向首先由 9.5%升高至 10.5%，然后逐渐降低至 6.0%。整体接头的抗拉强度达到母材的 88.5%。接头的主要强化机制为细晶强化。

关键词：显微组织演变；力学性能；强化机制；搅拌摩擦焊；镁合金；厚板

(Edited by Wei-ping CHEN)